Short-term and seasonal pH, pCO_2 and saturation state variability in a coral-reef ecosystem

Sarah E. C. Gray,[1] Michael D. DeGrandpre,[2] Chris Langdon,[3] and Jorge E. Corredor[4]

Received 16 May 2011; revised 15 June 2012; accepted 8 July 2012; published 11 August 2012.

[1] Coral reefs are predicted to be one of the ecosystems most sensitive to ocean acidification. To improve predictions of coral reef response to acidification, we need to better characterize the natural range of variability of pH, partial pressure of carbon dioxide (pCO_2) and calcium carbonate saturation states (Ω). In this study, autonomous sensors for pH and pCO_2 were deployed on Media Luna reef, Puerto Rico over three seasons from 2007 to 2008. High temporal resolution $CaCO_3$ saturation states were calculated from the in situ data, giving a much more detailed characterization of reef saturation states than previously possible. Reef pH, pCO_2 and aragonite saturation (Ω_{Ar}) ranged from 7.89 to 8.17 pH units, 176–613 μatm and 2.7–4.7, respectively, in the range characteristic of most other previously studied reef ecosystems. The diel pH, pCO_2 and Ω cycles were also large, encompassing about half of the seasonal range of variability. Warming explained about 50% of the seasonal supersaturation in mean pCO_2, with the remaining supersaturation primarily due to net heterotrophy and net $CaCO_3$ production. Net heterotrophy was likely driven by remineralization of mangrove derived organic carbon which continued into the fall, sustaining high pCO_2 levels until early winter when the pCO_2 returned to offshore values. As a consequence, the reef was a source of CO_2 to the atmosphere during the summer and fall and a sink during winter, resulting in a net annual source of 0.73 ± 1.7 mol m^{-2} year^{-1}. These results show that reefs are exposed to a wide range of saturation states in their natural environment. Mean Ω_{Ar} levels will drop to 3.0 when atmospheric CO_2 increases to 500 μatm and Ω_{Ar} will be less than 3.0 for greater than 70% of the time in the summer. Long duration exposure to these low Ω_{Ar} levels are expected to significantly decrease calcification rates on the reef.

Citation: Gray, S. E. C., M. D. DeGrandpre, C. Langdon, and J. E. Corredor (2012), Short-term and seasonal pH, pCO_2 and saturation state variability in a coral-reef ecosystem, *Global Biogeochem. Cycles*, *26*, GB3012, doi:10.1029/2011GB004114.

1. Introduction

[2] The oceans absorb approximately one third of the anthropogenic CO_2 emitted to the atmosphere [*Sabine et al.*, 2011]. While this CO_2 uptake helps ameliorate human-caused greenhouse warming, the amount of absorbed CO_2 is so massive that it is significantly changing the chemistry of the oceans [*Feely et al.*, 2004]. When CO_2 reacts with seawater it forms carbonic acid, lowering pH, carbonate ion concentration ($[CO_3^{2-}]$) and $CaCO_3$ saturation states [e.g., *Cao et al.*, 2007; *Fabry et al.*, 2008; *Orr et al.*, 2005]. This CO_2-driven "ocean acidification" has already decreased sea surface pH by more than 0.1 pH units since the beginning of the industrial revolution [*Caldeira and Wickett*, 2003]. Once anthropogenic CO_2 enters the oceans there is no practical way to remove it and the oceans will require thousands of years to naturally return to a higher pH state [*The Royal Society*, 2005; *Solomon et al.*, 2009].

[3] Increasing dissolved CO_2, described as the partial pressure of CO_2 (pCO_2), and decreasing pH will likely affect many marine organisms and alter ecosystem community structure [*Fabry et al.*, 2008; *The Royal Society*, 2005]. Corals and other calcifying organisms are particularly at risk due to their dependence on CO_3^{2-} concentration and $CaCO_3$ saturation states (Ω) [*Gledhill et al.*, 2008]. Laboratory tests have shown that as the pCO_2 of seawater is increased, coral $CaCO_3$ production begins to decline [*Jokiel et al.*, 2008; *Langdon et al.*, 2003; *Langdon and Atkinson*, 2005; *Leclercq et al.*, 2000]. These experiments provide insights into how corals may react to changing CO_2 levels, but it can be difficult to extrapolate the data to natural systems, in part because the natural range of the CO_2 system that corals are exposed to

[1]Environmental Sciences, Trinity College, Hartford, Connecticut, USA.
[2]Department of Chemistry and Biochemistry, University of Montana, Missoula, Montana, USA.
[3]Rosenstiel School of Marine and Atmospheric Sciences, University of Miami, Coral Gables, Florida, USA.
[4]Department of Marine Sciences, University of Puerto Rico, Mayagüez, Puerto Rico.

Corresponding author: M. D. DeGrandpre, Department of Chemistry and Biochemistry, University of Montana, 32 Campus Dr., Missoula, MT 59812, USA. (michael.degrandpre@umontana.edu)

0886-6236/12/2011GB004114

Figure 1. Location of Media Luna reef off the southern coast of La Parguera, Puerto Rico. Sample sites were located at the head (A) (17°56′17″N, 67°02′25″W) and tail (B and C) (17°56′19″N, 67°03′7″W and 17°56′7″N, 67°02′54″W) of Media Luna, with waters approximately 4 m deep at head site A and 5 and 4 m deep at tail sites B and C, respectively. All discrete samples reported here were collected at site A. The ICON mooring and deployments 1 and 2 were at site B. Deployment 3 was at site C. The distance from A to C is ~0.9 km.

is not well characterized. This lack of information is largely due to the difficulty of making CO_2 system measurements with sufficient duration and temporal resolution. Two of the inorganic carbon parameters, such as pCO_2, pH, total alkalinity (A_T) or total dissolved inorganic carbon (DIC), must be measured to calculate the seawater CO_2 system, including $CaCO_3$ saturation states, restricting most past studies to ship-based sampling. To obtain more continuous inorganic carbon system data for coral reefs, studies have used in situ potentiometric pH sensors [e.g., *Frankignoulle et al.*, 1996; *Gattuso et al.*, 1999; *Yates and Halley*, 2006; *Santos et al.*, 2011] and autonomous pCO_2 systems [e.g., *Kayanne et al.*, 2005; *Bates et al.*, 2001]. However, with a few exceptions [e.g., *Bates et al.*, 2001; *Drupp et al.*, 2011], these studies have been short duration (days to weeks). Consequently, there is a lack of long-term high temporal resolution pH, pCO_2, and Ω data for coral reefs.

[4] There now exists improved measurement technology that can be used for coral reef biogeochemical studies. The revitalization and improvement of the indicator-based pH method [*Byrne and Breland*, 1989] have made precise and accurate pH data available for CO_2 system calculations compared to past studies that used electrochemical pH measurements. Several in situ pH systems have now been developed based on the spectrophotometric pH methodology [*Liu et al.*, 2006; *Nakano et al.*, 2006; *Seidel et al.*, 2008]. The SAMI-pH, or Submersible Autonomous Moored Instrument for pH, is an indicator-based sensor capable of long-term, in situ pH measurements [*Martz et al.*, 2003; *Seidel et al.*, 2008; *Cullison Gray et al.*, 2011; *Emerson et al.*, 2011]. Recent studies have shown that $[CO_3^{2-}]$ and $CaCO_3$ saturation states can be accurately calculated from in situ pH and pCO_2 time series data [*Cullison Gray et al.*, 2011]. In this study, we deployed the SAMI-pH with the autonomous pCO_2 sensor SAMI-CO_2 [*DeGrandpre et al.*, 1995] in three separate seasons off the southern coast of Puerto Rico spanning the years 2007–2008. Our goals here are to report the observed diel to interseasonal range of reef pH, air-sea CO_2 fluxes, and $CaCO_3$ saturation states, evaluate the controlling processes, and compare our results with other studies.

2. Methods

2.1. Site Description

[5] Measurements were focused on Media Luna Reef in the La Parguera shelf reef system (Figure 1). The reef is a 1.5 km long, emergent shelf reef 3.3 km south of La Parguera, Puerto Rico and is adjacent to an extensive mangrove system [*Acevedo et al.*, 1989]. Water on the reef has primarily an oceanic source, with a general east to west current flow. The location was selected to take advantage of measurements being made at the NOAA Integrated Coral Reef Observing Network (ICON) buoy (site B, Figure 1). Media Luna met NOAA's requirements that the site be within a U.S. territory, have a bottom surface hard enough to drill into, be accessible for cleaning every ten days to two weeks and be located on the lee side from prevailing winds (J. Hendee, personal communication, 2009). The University of Puerto Rico, Mayagüez field station on Magueyes Island in La Parguera, Puerto Rico provides maintenance and research support for the buoy.

[6] Two sites were selected for this study, one at the head (upwind) and one at the tail of the reef, in order to characterize spatial variability and to determine if net calcification could be quantified along the reef. Three deployments spanning June 19–August 21, 2007, January 7–March 14, 2008, and September 16–November 21, 2008, are referred to as summer, winter and fall deployments, respectively. After examining current and salinity data from the second deployment, we determined that water from site A was not traveling directly to site B. For the third deployment, a new reef tail site was chosen (site C, Figure 1) so that the site would be directly in the mean flow path of water coming from site A.

2.2. Time Series Data

[7] Air and water temperature, salinity, photosynthetically active radiation (PAR), and wind velocity at 6.5 m were measured hourly on the NOAA ICON mooring. Water temperature, salinity and PAR sensors were located near the bottom at ~5 m depth. An ADCP (RD Instruments 1200 KHz Workhorse Monitor) was deployed at the reef head during the winter and fall periods. The SAMI-pH and SAMI-CO_2 sensors were deployed on the bottom at sites A and C and approximately 1 m from the bottom at the ICON site B (Figure 1). The sensors were programmed to make measurements every half hour. The SAMI-pH and SAMI-CO_2 are indicator-based sensors (Sunburst Sensors).

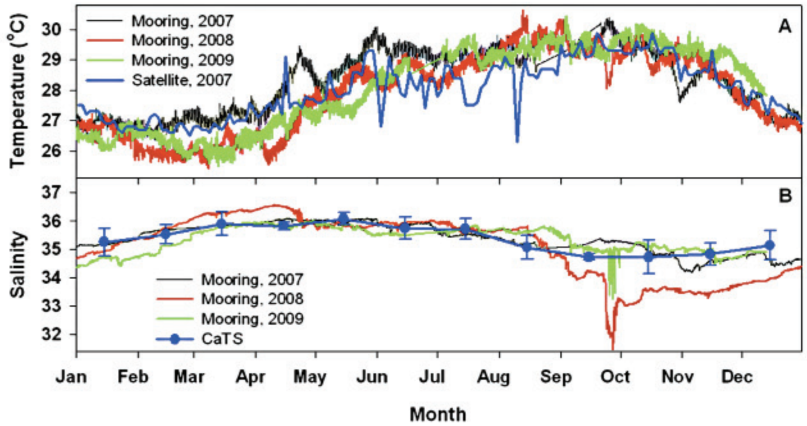

Figure 2. Temperature and salinity data from Media Luna reef and Caribbean Time Series (CaTS) (17.6°N, 67°W) locations. (a) Annual temperature record for reef site B from the NOAA ICON mooring (hourly) from 2007 to 2009 and from NOAA satellite data (every other day) for 2007 from the CaTS location. (b) Annual salinity record for reef site B from the NOAA ICON mooring (hourly) from 2007 to 2009 and from discrete CTD casts at CaTS (monthly average of points from 1993 to 1999, n ~ 5 for all months).

The SAMI-pH combines metacresol purple (mCP) indicator with a seawater sample to determine pH [*Martz et al.*, 2003; *Seidel et al.*, 2008]. The SAMI-pH accuracy was checked prior to deployment by comparison with UV-VIS measurements of seawater samples or with tris buffer in synthetic seawater [*DelValls and Dickson*, 1998]. These measurements found an accuracy ranging from 0.001 to 0.005 pH units and precision of ± 0.0006 pH units. In the SAMI-CO_2 sensor, CO_2 equilibrates across a silicone rubber membrane filled with bromothymol blue (BTB) indicator [*DeGrandpre et al.*, 1995]. The SAMI-CO_2s were calibrated with CO_2 gas mixtures, verified with an infrared CO_2 analyzer (LI-COR, LI-840A), and then checked for accuracy in a 200 L water tank. A membrane contactor (Membrana Liqui-Cel MiniModule) was used to equilibrate a flowing air stream with the CO_2 in the tank. The equilibrated air passed through a gas drier (Perma Pure), then into an infrared CO_2 analyzer (LI-COR, LI-840A) for detection. A bubbling stone, attached to a room air supply and a soda lime CO_2 trap, was used to drive down the CO_2 in the tank, when necessary. Based on these tests, accuracy of the SAMI-CO_2 is ~ 5 μatm with a precision of ± 1 μatm. Dissolved oxygen (Aanderaa 4175 Optode) was measured every half hour during the last two deployments. Oxygen sensors were calibrated in saturated and zero oxygen solutions before deployment. The O_2 sensors have an accuracy of ~ 8 μM based on the factory calibration with a resolution of <1 μM. Chlorophyll-a (chl-a) fluorescence was measured using an in situ fluorometer (Chelsea Instruments Minitracka) with chl-a concentration calculated from the factory calibration.

[8] Atmospheric pCO_2 was calculated from hourly dry mole fraction CO_2 at Mauna Loa atmospheric CO_2 time series station which is the closest in latitude (19°32′N) to the Media Luna sites at 17°56′N. Mole fraction was converted to pCO_2 using local reef barometric pressure and sea surface temperature (water vapor). Oceanic temperature and salinity data for the Caribbean Time Series (CaTS) location (17°36′N, 67°W) were used for comparison with the coastal data. Near daily resolution temperature data were derived from satellite data at CaTS using the NOAA Comprehensive Large Array-data Stewardship System (CLASS) for 2007. The salinity data from CaTS were measured using a conductivity-temperature-depth sensor (Sea-Bird Electronics SBE19 CTD) on a nearly monthly basis from 1993 to 1999 [*Corredor and Morell*, 2001].

2.3. Discrete Measurements

[9] Discrete samples were collected from the reef head (A) and reef tail (B or C) once or twice a day during the first 1–2 weeks of each deployment, as well as several other times throughout the deployment to verify sensor measurement data quality and provide additional data for interpretation of the in situ time series. Samples were collected using a Van Dorn horizontal water sampler (Wildco) and were stored in the dark at room temperature until analyzed. A_T samples were analyzed within 24 h by open-cell potentiometric titration following DOE procedure SOP3b [*Dickson et al.*, 2007] using a custom-built automated Gran titration system [*Langdon et al.*, 2000]. Alkalinity certified reference materials (CRMs) [*Dickson et al.*, 2003] were used to standardize the HCl titrant. Accuracy and precision of field samples was ± 1.5 μmol kg^{-1}. pH was measured spectrophotometrically on the total pH scale within 8 h of collection on a UV-VIS spectrophotometer (Shimadzu UV-1601) following DOE procedures [*Clayton and Byrne*, 1993; *Dickson et al.*, 2007]. Precision was ± 0.003 pH units. During the third (fall) deployment, tris seawater buffers [*DelValls and Dickson*, 1998] became available to assess the accuracy of the UV-VIS pH measurements. The accuracy was 0.0061 ± 0.0023 pH units. Discrete pCO_2, calculated from A_T and pH data, was used to quality control the in situ pCO_2. Oxygen samples were analyzed using the Winkler titration method [*Culberson and Huang*, 1987]. The comparison between sample and in situ measurements is presented in the Results.

2.4. CO_2 Equilibrium and Temperature Calculations

[10] All CO_2 system calculations were performed using CO2SYS [*Pierrot et al.*, 2006] with K_1 and K_2 from *Mehrbach et al.* [1973] refit by *Dickson and Millero* [1987], KSO_4 from *Dickson* [1990] and pH on the total scale.

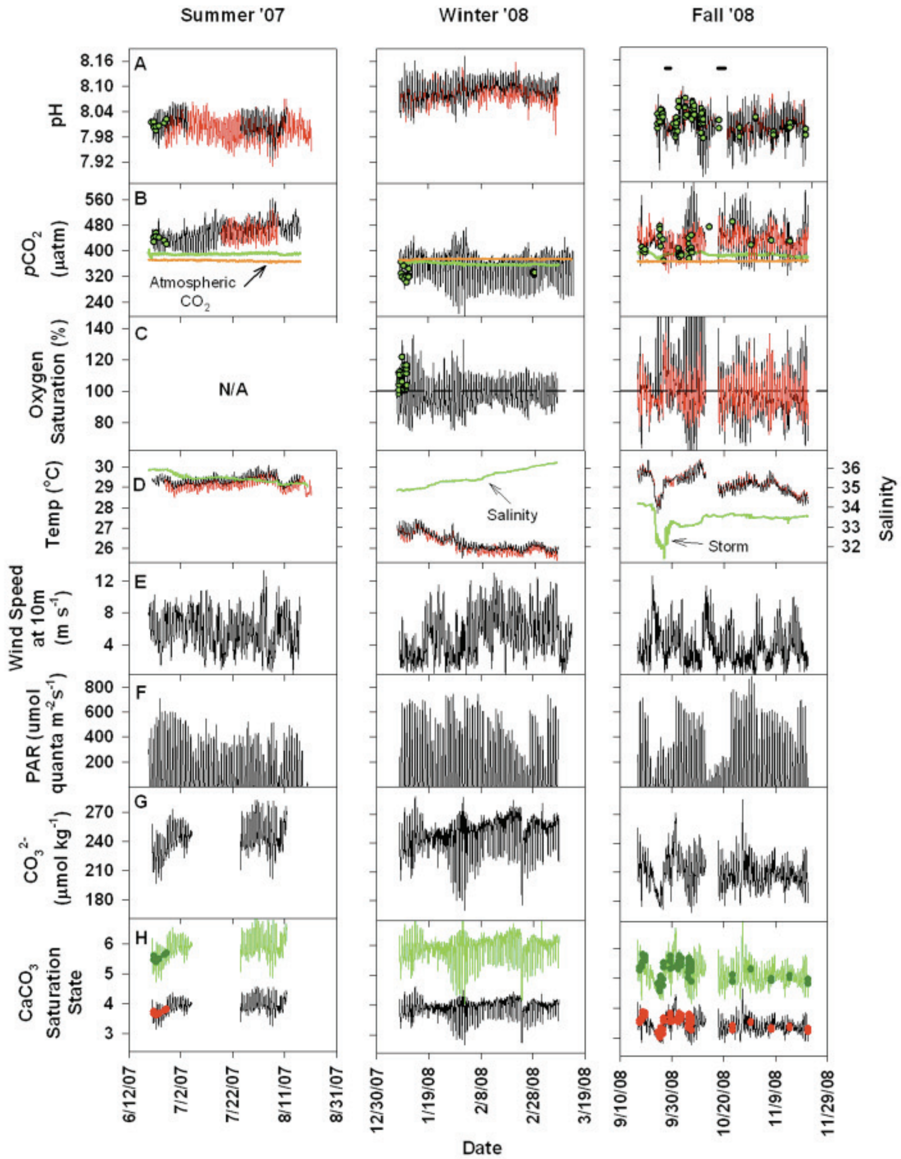

Figure 3. Compilation of time series data from Media Luna reef (summer 2007, left; winter 2008, center; fall 2008, right). (a) pH (total scale) from the SAMI-pH at the reef head (black) and reef tail (red) and from discrete pH samples (green circles). The bold black bars in Figure 3a, fall '08 show the times when storms passed over PR. (b) pCO_2 from the SAMI-CO_2 at the reef head (black) and reef tail (red) and pCO_2 calculated from samples (green circles). The red line shows the average atmospheric pCO_2 value from Mauna Loa (369 μatm). The green line shows estimated open ocean pCO_2 at the reef temperature, calculated using the relationship of *Olsen et al.* [2004]. (c) Dissolved O_2 at the reef head (black) and reef tail (red) and from O_2 samples (green circles). No O_2 sensors were deployed during summer 2007. The dashed black line shows 100% O_2 saturation. (d) Temperature from the SAMI-pH at the reef head (black) and tail (red) and salinity (green) from the NOAA ICON mooring at the reef tail site B. (e) Wind speed from the ICON mooring at reef tail site B corrected to 10 m. (f) Photosynthetically Active Radiation (PAR) from the ICON mooring at the reef tail site B. (g) Carbonate concentrations calculated from pH and pCO_2 data. (h) Aragonite (black) and calcite (green) $CaCO_3$ saturation states calculated from pH and pCO_2 data. Values calculated from discrete measured pH and A_T are also shown (calcite in green circles, aragonite in red circles).

Temperature effects were examined using CO2SYS by inputting pH and pCO_2 using the in situ temperature and salinity, with the program set to output the pH and pCO_2 at the mean annual temperature (28°C).

2.5. Calcium Carbonate Saturation States

[11] Saturation states were calculated in CO2SYS using $\Omega = [Ca^{2+}][CO_3^{2-}]/K_{sp}$ where K_{sp} is the temperature, pressure and salinity dependent solubility product constant.

Table 1. Average Water Column Value of Each Time Series Parameter by Season at the Reef Head (Site A)[a]

Parameter	Summer 2007	Winter 2008	Fall 2008
Temperature (°C)	29.3 ± 0.2 0.41	26.3 ± 0.4 0.45	29.1 ± 0.5 0.53
Salinity	35.8 ± 0.22 0.08	35.2 ± 0.35 0.04	33.8 ± 0.50 0.10
pH	8.01 ± 0.02 0.079	8.09 ± 0.02 0.067	8.00 ± 0.03 0.093
pCO_2 (μatm)	460 ± 33 77	356 ± 43 130	437 ± 44 130
A_T (μmol kg^{-1})	2315 ± 6 ND	2295 ± 39 ND	2223 ± 30 ND
DIC (μmol kg^{-1})	1996 ± 10 ND	1974 ± 32 ND	1921 ± 21 ND
O_2 saturation (%)	ND	97.5 ± 9.5 28.6	101.6 ± 22 60.6
CO_3^{2-} (μmol kg^{-1})	238 ± 17 41	250 ± 16 53	209 ± 16 43
Aragonite saturation	3.94 ±0.24 0.64	3.94 ± 0.25 0.83	3.42 ± 0.26 0.72
Calcite saturation	5.90 ± 0.36 0.95	5.95 ± 0.38 1.25	5.13 ± 0.39 1.08

[a]The mean diel range is shown below each average. A_T is from all available discrete samples and DIC is calculated from pH and A_T from all available discrete samples (reef head and tail). ND = no data.

$[Ca^{2+}]$ was determined using its known relationship with salinity, whereas $[CO_3^{2-}]$ was calculated from two measured inorganic carbon parameters. In *Cullison Gray et al.* [2011], we showed that in situ pH and pCO_2 data can be used to accurately calculate $[CO_3^{2-}]$ and Ω. We use the high-resolution pH and pCO_2 time series presented here to characterize reef aragonite (Ω_{Ar}) and calcite (Ω_{Ca}) saturation states with unprecedented detail.

2.6. Air-Sea Flux Calculations

[12] The air-sea CO_2 flux was estimated using $F_{GAS} = kS\Delta pCO_2$, where k is the gas transfer velocity, S is the gas solubility and ΔpCO_2 is the difference in pCO_2 between the surface ocean and the atmosphere. A negative F_{GAS} represents a flux from the atmosphere to the ocean. The gas transfer velocity was estimated using the wind speed relationship of *Ho et al.* [2006]. Tidal currents can affect gas transfer rates in shallow coastal and estuarine locations [*Borges et al.*, 2004] but was not likely to be important in this area because of the small tidal range (max of ~0.4 m). The net annual flux was calculated from pCO_2 interpolated between seasons with k from hourly winds at the NOAA ICON site corrected to 10 m [*Large et al.*, 1995].

3. Results

3.1. Reef Hydrography

[13] Hydrographic data from the open ocean CaTS site, located 52 km south of Puerto Rico (17°36′N, 67°W), and Media Luna reef are compared in Figure 2. The reef temperature and salinity records are in general very similar to the CaTS site, indicating that local processes, with exceptions noted below, do not significantly alter the T and S of the open ocean source water. These data also show that the period of our study is, at most times, representative of typical conditions on the reef, based on comparison with the ICON Media Luna data from other years. CTD casts conducted throughout the study indicated the entire water column over the reef was always well mixed. Current meter measurements showed that the mean water flow across the reef was toward the west-southwest (from sites A to C, Figure 1). Tides were diurnal with water depth changes between 0.05 and 0.4 m.

3.2. Data Overview

[14] Data for all three deployments are shown in Figure 3. Gaps in the fall pH, pCO_2, O_2 and temperature data correspond to when the instruments were removed from the reef preceding severe weather. For an unknown reason, the winter sample pH data did not closely match the in situ pH values. Because the SAMI-pH and discrete A_T combination produced reasonable pCO_2 values compared to the SAMI-CO_2 (Figure 3b), the winter sample pH values were not used. The SAMI-pH and SAMI-CO_2 and the discrete samples, excluding the winter pH, matched to within +0.0006 ± 0.0082 pH units (n = 86) and −1 ± 14 μatm (n = 86), respectively, reported as the mean difference ± standard deviation of the difference. No offsets were applied to the SAMI pH data; however, pCO_2 data were corrected to the discrete (calculated) pCO_2 when offsets were present. Only constant offsets were applied and there was no detectable drift. The difference between the O_2 optodes and discrete Winkler O_2 measurements was −0.6 ± 3.7% saturation (n = 28); no offsets were applied to the O_2 data. The pH-pCO_2 derived $CaCO_3$ saturation states (Figure 3h) compared well with those calculated from discrete pH and A_T with differences of −0.002 ± 0.14 (n = 75) for aragonite and −0.002 ± 0.20 (n = 75) for calcite. Random spatial and temporal mismatches between sampling and in situ measurements likely contributed to the relatively large standard deviations between in situ and discrete biogeochemical data sets.

[15] The mean data ranges in Figure 3 are given in Table 1. Over the three deployments, temperature and salinity ranged from 25.5 to 30.7°C and 31.4–36.3, respectively. Oxygen saturation varied from 62 to 138%. Reef pH and pCO_2 were between 7.89 and 8.17 pH units and 176–613 μatm, respectively, with the lowest pH and highest recorded pCO_2 in the fall. The ranges of pH and pCO_2 were dominated by the seasonal cycle but the diel ranges were also large, at times encompassing the seasonal pH range (Table 1) and extending the pH minimum to ~7.89 for a short period in October (Figure 3). The diel ranges were largest in the fall. The Ω_{Ar} and Ω_{Ca} ranged from 3.0–4.4

Table 2. R^2 Correlations Between pH and Other Parameters[a]

Season	T	S	D	pCO_2	O_2	Ω_{Ar}
summer ’07	0.004	0.02	0.07	0.46	ND	0.73
winter ’08	0.006	0.06	0.08	0.75	0.40	0.001
fall ’08	0.06	0.01	0.23	0.83	0.50	0.60

[a]For summer, pH, temperature (T), salinity (S), and depth (D) are from site B and pCO_2 is from site A (Figure 1). For winter and fall, all parameters are from site A except salinity and depth, which are from site B. ND = no data.

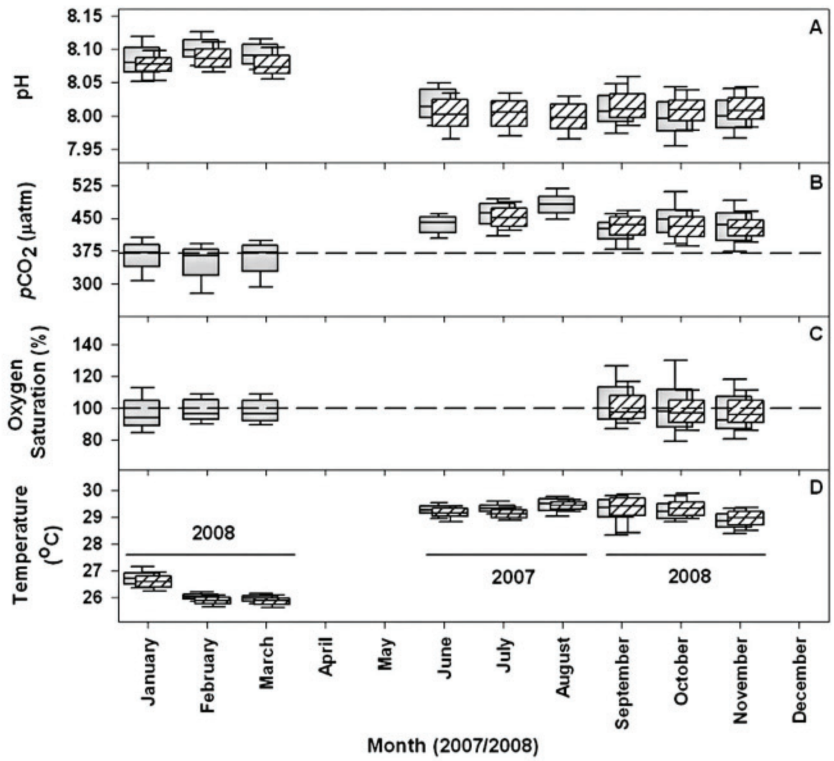

Figure 4. (a–d) Monthly means showing spatial difference between the reef head and tail over an annual cycle. Data in gray are from reef head site A. Data in white with diagonal hatching are from reef tail site B for Jan-Aug. and reef tail site C for Sept-Nov. Head and tail data are offset in time for clarity. Mean atmospheric pCO_2 is shown in Figure 4b (dashed line). For each box the centerline is the monthly median, the top and bottom of each box are the 75th and 25th percentiles and the top and bottom whiskers are the 90th and 10th percentiles. Years when data were collected are indicated in Figure 4d.

and 4.3–6.8, respectively and changed by 0.64–0.83 and 0.95–1.08, respectively, over a diel cycle.

[16] Because of the interest in understanding how ocean pH relates to other measured parameters, correlations with pH, by season, are shown in Table 2. The highest pH correlations were found with pCO_2 and Ω_{Ar}. The lower correlation between pH and pCO_2 for the summer season is likely due to the use of pH from the reef tail site B and pCO_2 from reef head site A, which was necessary due to missing data at the corresponding sites (Figure 3). Winter pH and Ω_{Ar} do not correlate indicating that pH is not always a good predictor of saturation states. The pH, pCO_2 and Ω_{Ar} relationships are discussed in more detail in Section 4.5. There was no evidence of a biogeochemical signal associated with the tidal cycles (depth in Table 2).

[17] Small biogeochemical and temperature gradients existed between the reef head and tail (Figure 3). Spatial differences are more clearly shown by comparing the monthly means (Figure 4) and seasonal averages (Table 3). There were larger differences during the first two deployments (summer, winter) when the sensors were located on opposite sides of the reef (Figure 1). At times large differences between sites A and C (fall) were observed, with the largest deviations in pH and pCO_2 occurring soon after tropical storms Kate (September 21–23) and Omar (October 14–17) (Figure 3). Site A, which is not sheltered by nearby emergent reefs like the tail sites (Figure 1), may be more directly influenced by terrestrial inputs during these storm periods (also see section 4.1 below). While our hope was to quantify biogeochemical rates of change across the reef using the pH, pCO_2, O_2 and current (ADCP) data (essentially the pH-A_T technique) [e.g., *Gattuso et al.*, 1999], the small differences during the winter relative to the large error in calculated A_T [*Cullison Gray et al.*, 2011] and failure of the ADCP in the fall (the ADCP was not deployed in the summer), prevented this. The spatial data do show, however, that the local water is not strongly influenced by a single reef and that the observed biogeochemical changes are, in general, representative of the broader reef-shelf system. To simplify the discussion that follows, the data collected at the reef head (site A, Figure 1) are primarily used and data at the

Table 3. Average Difference Between the Media Luna Reef Head and Tail Sites (Head-Tail) for Each Measured Parameter by Season[a]

Parameter	Summer 2007	Winter 2008	Fall 2008
pH (pH units)	0.011 ± 0.022	0.012 ± 0.021	-0.008 ± 0.018
pCO_2 (μatm)	24.0 ± 26.2	—	6.0 ± 28.4
O_2 Saturation (%)	—	—	6.9 ± 26.5
Temperature (°C)	0.2 ± 0.1	0.1 ± 0.1	-0.04 ± 0.08

[a]Lines indicate that data was not available at one or both sites.

reef tail are only discussed when data at the reef head were not available (see black and red traces in Figure 3).

4. Discussion

4.1. Comparison of pH With Other Reef Systems

[18] The large range of short-term and seasonal pH and pCO_2 variability on Media Luna reef (Table 1) appears to be typical of coral reefs [*Kayanne et al.*, 2005; *Yates and Halley*, 2006; *Manzello*, 2010; *Santos et al.*, 2011]. Here we highlight data specifically for pH because it is one of the most commonly measured inorganic carbon parameters and because of the pH connection to ocean acidification. Saturation states are discussed below. *Kayanne et al.* [2005] measured pH over an entire year with a pH sonde on a fringing reef (1.5–2.5 m depth) off Ishigaki Island, Japan and reported an average diel change of ~0.5 pH units (7.9–8.4) and a seasonal pH change of ~0.1–0.2 pH units. *Manzello* [2010] found a pH range of 7.65–8.26 for upwelling-impacted reefs located in the eastern Pacific Ocean. Reef pH was recorded over 24–48 h periods, approximately monthly, from 2000 to 2002 by *Silverman et al.* [2007]. Over the two-year period, the monthly pH average in the Red Sea reef lagoon (1.5–1.8 m water depth) varied by 0.1 pH units, from 8.2 to 8.3 pH units. The higher pH range found in this reef ecosystem is controlled by the high A_T in the Red Sea. In *Santos et al.* [2011], the diel pH ranged from 7.7 to 8.4 at Heron Island on the Great Barrier Reef. The large diel pH range found in reefs is dominated by primary production that is supported by the reef community [*Kleypas et al.*, 2011]. In La Parguera, the productivity of the reef has been affected by frequent coral bleaching since the mid-1980s, with an increase of 0.7°C in the maximum summer temperature from 1966 to 1995 [*Winter et al.*, 1998; *García et al.*, 1998]. Moreover, reefs on the southern coast of Puerto Rico have shown decreased species diversity and coral cover due to terrestrial sediment inputs [*Acevedo et al.*, 1989]. These impacts have likely resulted in decreased pH and pCO_2 variability compared to healthy reefs [*Kayanne et al.*, 2005].

4.2. Sources of Biogeochemical Variability

4.2.1. Physical Processes

[19] Here we evaluate processes that control pH and pCO_2 variability. Saturation state variability is evaluated separately in section 4.5. As shown in Table 2, the pH was not correlated with temperature, salinity or depth (tides). Although heating and cooling are typically important contributors to pH and pCO_2 variability, and on Media Luna reef there is a significant increase in temperature from winter to summer (Figure 3d), the temperature correlation is weak because other sources of variability muddle the relationship (discussed below in this section). To separate out the temperature forcing, the pH and pCO_2 time series data were recalculated at a constant temperature (28°C), as described in section 2.4. The temperature adjusted data indicate that 50%, or 0.04 pH units, of the 0.08 pH unit seasonal change (Table 1) and 46%, or 48 μatm, of the 104 μatm seasonal pCO_2 change (Table 1) were due to warming from winter to summer, with a similar magnitude but in the opposite direction from fall to winter.

[20] Variations in source water inputs, net community production (NCP = gross primary production – net community respiration), $CaCO_3$ production/dissolution and air-sea gas exchange could also contribute to the observed variability. We can estimate the oceanic source water pCO_2 using an empirical SST-pCO_2 relationship developed by *Olsen et al.* [2004] for the oligotrophic Caribbean Sea. Their temperature, latitude and longitude-dependent relationships were developed using shipboard pCO_2 and remotely sensed sea surface temperature measured in the Caribbean Sea for the year 2002. This relationship was used with the local SST and location of the reef head to estimate the oceanic source water pCO_2. We added the difference in the annual mean atmospheric pCO_2 at Mauna Loa between 2002 and 2007 (10.6 μatm) to the calculated pCO_2 to estimate the 2007 open ocean values, assuming the surface ocean pCO_2 tracks the atmospheric CO_2 increase. Mean summertime offshore pCO_2 was 390 ± 2.5 μatm, or about 70 μatm below the mean summer reef pCO_2 (Figure 3b and Table 1). During the winter, the estimated mean offshore pCO_2 was 359 ± 4 μatm, very close to the reef mean of 356 μatm, while the fall offshore pCO_2 (388 ± 4.6 μatm) was again well below the reef mean (437 μatm). The seasonal temperature range on the reef and open ocean are very similar, as shown in Figure 2 but, using CO2SYS, the seasonal range of the offshore water pCO_2 shown in Figure 3 is mostly explained by temperature (i.e., the *Olsen et al.* [2004] algorithm is primarily driven by the thermodynamic pCO_2 variability), in contrast to the reef where, as shown above, only ~50% of the observed seasonal range is due to seasonal heating and cooling. It is clear that the biogeochemical properties of offshore waters traversing the insular shelf are strongly imprinted by local processes. These observations are similar to those of *Bates et al.* [2001], where the local reef profoundly alters the open ocean biogeochemical composition.

[21] The monthly mean values are compared to the temperature-corrected data in Figure 5. The constant temperature pCO_2 is near atmospheric saturation in the winter (Figure 5b) whereas in the summer and fall it is significantly above saturation. As described by *Takahashi et al.* [2002], this "residual" constant temperature pCO_2 represents contributions from water mass changes, air-sea gas exchange and biological processes. In the summer, when the reef water strongly resembles offshore water (based on temperature and salinity; Figure 2), only biological processes could generate the observed supersaturation; whereas in the fall there is significant freshwater input that could alter the inorganic carbon system. Straight dilution has negligible effects on pH and pCO_2, estimated by decreasing the seasonal DIC and A_T (Table 1) in direct proportion to salinity and recalculating in COSYS. Therefore, the fall supersaturation also requires some other explanation. These processes are discussed in the following section.

4.2.2. Biological Processes

[22] In this discussion biological variability is assumed to originate from NCP and calcification within the sediments, water column and corals. Calcification can be estimated by quantifying changes in A_T over time [e.g., *Gattuso et al.*, 1999]. We compared the balance between the open ocean and reef A_T measured on discrete samples. Open ocean A_T was calculated from the temperature-salinity relationship of *Lee et al.* [2006] using T and S at the CaTS site shown in Figure 2. Because our A_T measurements are not for a single year, these calculations assume that changes in A_T are consistent from year to year.

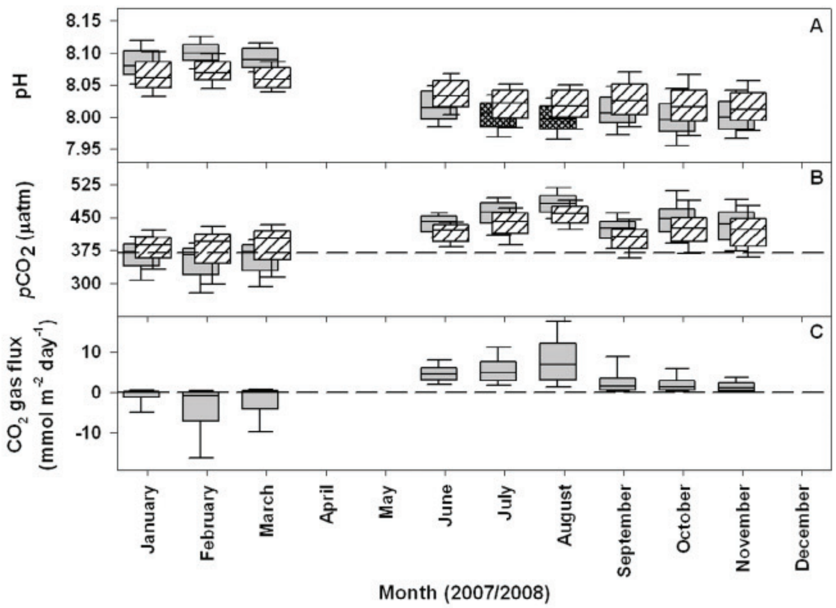

Figure 5. (a–c) Monthly means over an annual cycle (gray) with temperature-corrected data (diagonal white hatched, offset in time for clarity). All data in Figures 5a–5c are from the reef head site A with the exception of the July and August pH data (shown in dark crosshatch), which are from the reef tail site B. The annual mean temperature of 28°C was used for the temperature-corrected data. Mean atmospheric pCO_2 is shown in Figure 5b (dashed line). In Figure 5c, the dashed line shows the zero gas flux line. For each box the centerline is the monthly median, the top and bottom of each box are the 75th and 25th percentiles and the top and bottom whiskers are the 90th and 10th percentiles.

[23] The offshore calculated A_T is primarily dependent upon salinity, i.e., the *Lee et al.* [2006] relationship has a weak temperature dependence, with increasing A_T throughout the winter, leveling off in the spring, decreasing in the late summer and increasing again in the late fall (Figure 6). These changes in A_T (or salinity) are in response to seasonal rainfall, evaporation and freshwater inputs from the Amazon and Orinoco Rivers [*Corredor and Morell*, 2001]. The reef A_T was similar to offshore levels in the winter and spring but dropped below them in the summer. The large drop in late September corresponds to a period of intense rain (~20 cm in 12 h) associated with tropical storm Kate. The differences between the salinity-normalized A_T (= $35xA_T$/salinity) for the reef and offshore waters can indicate $CaCO_3$ formation or dissolution on the reef. From January to June, the salinity-normalized A_T at the offshore site decreased 3 μmol kg^{-1}, due to the temperature dependence of the *Lee et al.* [2006] relationship. The salinity-normalized reef A_T decreased 31 μmol kg^{-1}, or a net calcification-driven A_T decrease of -28 μmol kg^{-1}. During the fall, salinity-normalized reef A_T for late September was significantly higher than offshore values (maximum mean difference was +57 $\pm$ 9 μmol kg^{-1}) (Figure 6). The high salinity-normalized A_T could either be generated by $CaCO_3$ dissolution or terrestrial (karst) inputs of A_T as a result of the September rainstorm. Any freshwater inputs with nonzero A_T will increase salinity-normalized A_T, as observed in other coastal areas [e.g., *Kawahata et al.*, 2000].

[24] These seasonal A_T changes were used to calculate the pH and pCO_2 changes due to calcification/dissolution, by assuming that the change in DIC:A_T stoichiometry is 0.5. The change in A_T and DIC were added to the initial A_T and

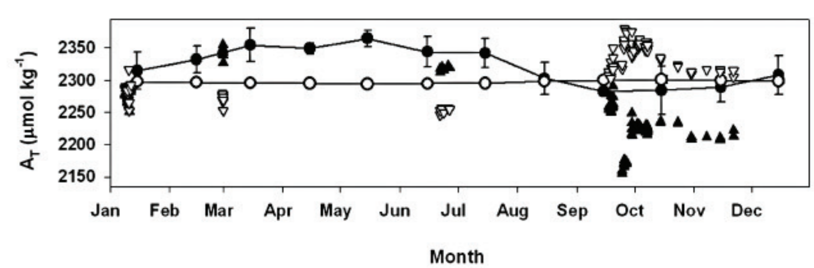

Figure 6. Annual cycle of A_T for the Media Luna reef and the open ocean. Filled black circles are monthly averaged A_T for the offshore CaTS site calculated from the *Lee et al.* [2006] relationship. Open circles are the monthly averaged CaTS A_T normalized to a salinity of 35. Filled black triangles show measured discrete A_T from the Media Luna reef head. Open triangles show Media Luna A_T normalized to a mean salinity of 35.

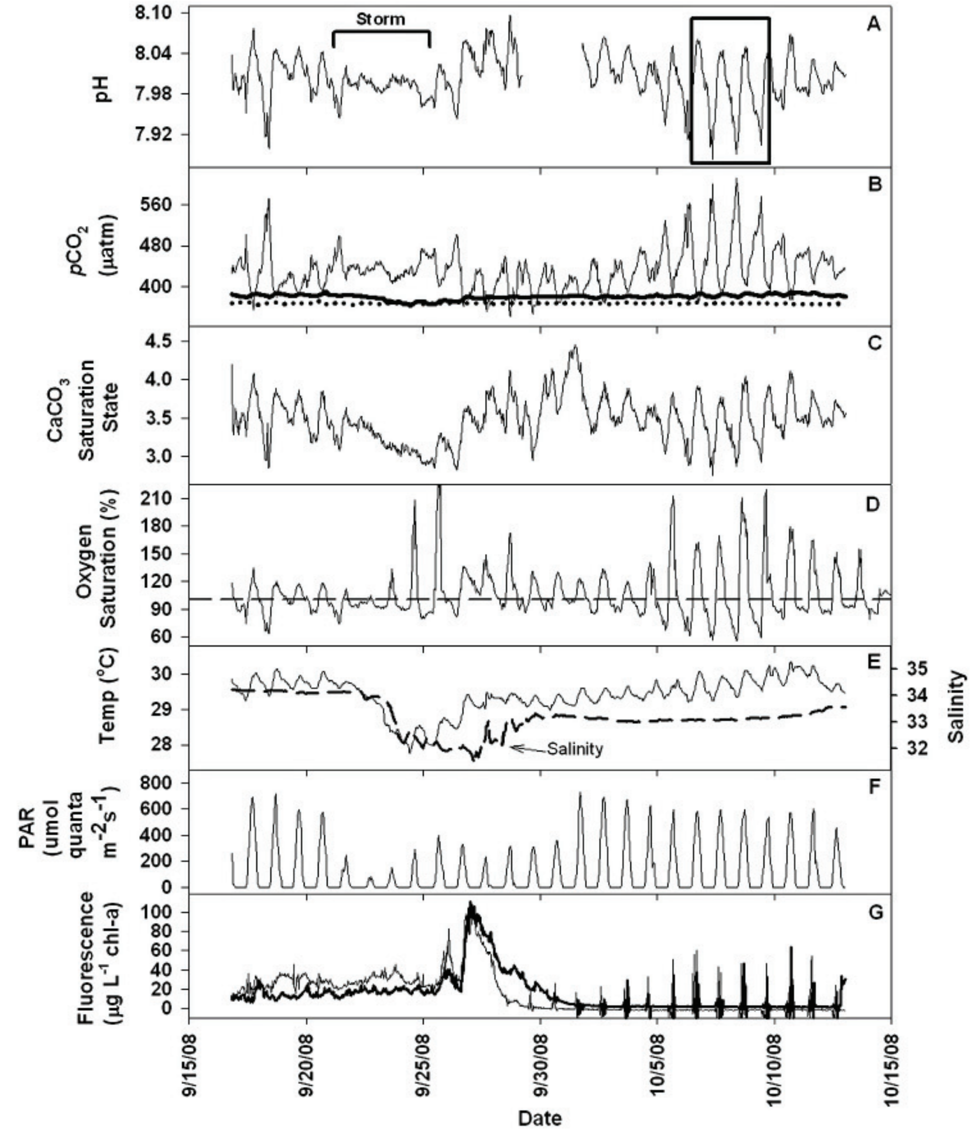

Figure 7. Blowup of the short-term data before and after tropical storm Kate (Sept 21–23, 2008). (a) pH from the SAMI-pH at the reef head. The black bracket shows the storm period and the black box shows the large diel changes after the storm. The gap in the pH data is due to instrument problems. (b) pCO_2 from SAMI-CO_2 at the reef head. The dotted line shows the average atmospheric CO_2 value from Mauna Loa (pCO_2 = 369 μatm). The thick black line shows estimated open ocean pCO_2 at the reef temperature, calculated using the relationship of *Olsen et al.* [2004]. (c) Aragonite saturation state. (d) Dissolved O_2 at the reef head. The dashed line shows 100% O_2 saturation. (e) Temperature (thin black) from the SAMI-pH and salinity (thick black) from the ICON mooring at the reef tail site B. (f) Photosynthetically Active Radiation (PAR) from the ICON mooring at the reef tail site B. (g) Chl-a concentration from head (thin black line) and tail (heavy black line). The spikes later in the record are believed to be caused by sunlight interference.

DIC for each season, with DIC values estimated using CO2SYS and the pH, A_T, T and S from discrete sample data at that time. The winter to summer pH and pCO_2 changes that resulted from the 28 μmol kg^{-1} decrease of A_T are -0.018 pH units and +15 μatm. In the fall, if the increase in salinity-normalized A_T was solely due to $CaCO_3$ dissolution, the pCO_2 would decrease by $\sim$30 μatm. Alternatively, if the source of A_T was runoff accompanied by DIC, pCO_2 would increase by $\sim$20 μatm, assuming that the DIC increased the same amount as A_T, i.e., A_T was 100% bicarbonate alkalinity. The lower mean pCO_2 observed in September (Figure 5) suggests that $CaCO_3$ dissolution was the dominant process perhaps brought on by the large freshwater input and net respiration (see in this section below).

[25] Of the winter to summer pH and pCO_2 changes shown in Table 1 and Figure 5, -0.02 pH units and 41 μatm could not be accounted for by heating and calcification. The remaining unexplained summer and fall pCO_2

Table 4. Air-Sea CO_2 Fluxes[a]

Data Source	Summer 2007	Winter 2008	Fall 2008	Annual (mol m^{-2} $year^{-1}$)
Media Luna pCO_2 time series	6.3 ± 4.7	−2.9 ± 5.6	2.2 ± 2.6	0.73 ± 1.7
Olsen et al. [2004]	0.85 ± 0.78	−2.0 ± 2.0	0.41 ± 0.59	−0.04 ± 0.43

[a]Negative values are a flux from the atmosphere into the ocean. Seasonal fluxes are in mmol m^{-2} day^{-1}. *Olsen et al.* [2004] fluxes were calculated using pCO_2 predicted from their relationships, using the temperature at Media Luna reef, adjusted for changes in atmospheric pCO_2 (see text). The annual *Olsen et al.* [2004] value is calculated from the continuous temperature data whereas the Media Luna flux is calculated using all of the time series data with data interpolated between seasons.

supersaturation likely originated from net respiration of organic carbon. The southwestern coast of Puerto Rico contains 995 ha of mangroves, as well as several offshore mangrove colonies on emergent portions of the reef [*Cintrón et al.*, 1978; *García et al.*, 1998]. Mangrove-derived organic carbon can subsequently be remineralized leading to high pCO_2 values as observed in other coastal areas [*Borges et al.*, 2003, 2005; *Bouillon et al.*, 2007; *Chen and Borges*, 2009; *Koné and Borges*, 2008]. At Media Luna reef, organic carbon inputs from adjacent mangroves and seagrass beds would need to be high in the summer and fall and low in the winter to account for the difference between pCO_2 levels. *Koné and Borges* [2008] found higher pCO_2 during the summer to fall rainy season and lower pCO_2 during the winter to spring dry season in waters with surrounding mangrove forests. At Media Luna reef, average January rainfall is <10% of that during the summer and fall months, supporting the seasonality of mangrove-derived organic matter input.

[26] To summarize the observed seasonal changes, the summer pCO_2 supersaturation can be broken down to ~46% heating/cooling, 14% net calcification, and 40% net respiration. In the fall, pCO_2 and pH likely return to winter levels through net dissolution of $CaCO_3$, net gas exchange to the atmosphere, along with a decrease in mangrove-derived organic carbon fluxes. Net production could also play an important role in the fall to winter decline. However, net production could not be discerned from water mass movement as the mean CO_2 characteristics of the reef water begins to more closely resemble the offshore values during this transition (see 2008 salinity record in Figure 2 and winter pCO_2 in Figure 3b).

4.3. Short-Term Processes

[27] While seasonal changes were large, short-term (primarily diel) processes were also important in establishing the range of biogeochemical variability on the reef. We looked more closely at the short-term variability before and after tropical storm Kate (September 21–23) both to further show the effects of organic matter input discussed above and to examine the dynamics of the diel cycle on the reef (Figure 7). First, and this is consistent throughout the time series data, pH and O_2 concentration increased and pCO_2 decreased during the day, showing that calcification and heating/cooling (for pH and pCO_2) were secondary to primary production for controlling the diel cycles of pH and pCO_2 on the reef [*Kleypas et al.*, 2011]. It can be seen that both temperature and salinity dropped sharply during and after the storm (Figure 7e) and that low light levels (Figure 7g) initially led to a dramatic decrease in the diel variability of pH, pCO_2 and O_2. Approximately one week after this rain event a large algal bloom occurred which initially increased pH and drew down the pCO_2, similar to post-storm blooms observed on other reefs [*Drupp et al.*, 2011]. After September 30 the salinity stabilized and the mean and diel amplitude of pCO_2 increased rapidly (and mean O_2 decreased) suggesting that over the next few days net respiration primarily drove these changes. During this period, the pH reached its lowest recorded level (7.89 pH units) and had a diel range as large as 0.167 pH units. For comparison, the offshore source water pCO_2 is estimated to have very small diel variability with pCO_2 increasing by an average of ~4 ± 1.5 μatm from heating during the day [*Olsen et al.*, 2004]. The observed diel pCO_2 cycle on the reef is typically larger than the source water diel cycle by more than an order of magnitude and, because of the biological signal, is in the opposite direction. The effects on Ω_{Ar} are also shown (Figure 7c) with Ω_{Ar} dropping to ~3 during the periods of high freshwater input and high rates of respiration (low pH, high pCO_2). The seasonal sources of variability on Ω_{Ar} are discussed in section 4.5.

4.4. CO_2 Gas Flux

[28] The mean seasonal and annual CO_2 gas fluxes were calculated to determine if Media Luna reef was a net source or a sink of CO_2 to the atmosphere. As shown in Table 4 and Figure 5d, the reef was a source of CO_2 to the atmosphere during summer and fall and a sink in the winter, controlled by the processes discussed above. It was a net source of CO_2 to the atmosphere over an annual period, with a flux of +0.73 ± 1.7 mol m^{-2} $year^{-1}$. By comparison, the annual flux using the *Olsen et al.* [2004] pCO_2 was −0.04 ± 0.43 mol m^{-2} $year^{-1}$ (Table 4). While the offshore source water has a negligible CO_2 flux, seasonal heating, organic matter remineralization and net calcification make the reef a significant CO_2 source. A compilation of five coral reef systems by *Fagan and Mackenzie* [2007] showed net release of CO_2 to the atmosphere between +1.2 and +1.8 mol m^{-2} $year^{-1}$ with the exception of one reef near equilibrium (+0.1 mol m^{-2} $year^{-1}$).

4.5. $CaCO_3$ Saturation States

[29] The high resolution Ω_{Ar} and Ω_{Ca} time series are shown in Figure 3h, the seasonal means in Table 1, and the monthly mean Ω_{Ar} in Figure 8. The range of Ω_{Ar} at Media Luna falls within the middle range found for other reefs, with higher Ω_{Ar} in the high A_T system of *Silverman et al.* [2007] and lower Ω_{Ar} (commonly less than 3.0) in coral reefs exposed to upwelling [*Manzello*, 2010] and other reefs [*Shamberger et al.*, 2011; *Bates et al.*, 2010].

[30] One of the major seasonal features in the Media Luna data is that Ω_{Ar} was very similar from winter to summer but dropped significantly in the fall – a surprising difference because the pH and pCO_2 are more similar in the summer and fall. While the same processes that control pH and pCO_2

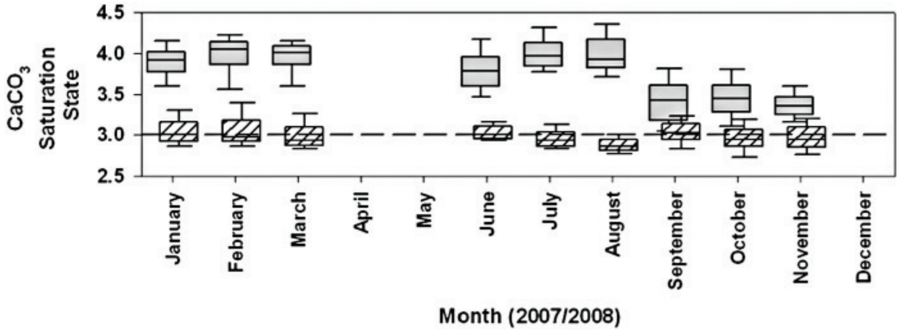

Figure 8. Monthly means of aragonite saturation state (plain gray boxes) at reef head site A over an annual cycle. Crosshatched white boxes represent the projected aragonite saturation if pCO_2 values increase to 500 μatm. For each box the centerline is the monthly median, the top and bottom of each box are the 75th and 25th percentiles and the top and bottom whiskers are the 90th and 10th percentiles.

on the reef will regulate Ω_{Ar} and Ω_{Ca}, there are some important differences. The summer Ω saturation states are close to the winter values (Figure 8 and Table 1) despite the summer's significantly lower pH and higher pCO_2 (Figure 3 and Table 1). Summer saturation states could be expected to be lower because of terrestrial organic matter remineralization that reduces pH and elevates pCO_2 as discussed above; however, the mean $[CO_3^{2-}]$ is similar for both seasons (Table 1). Seasonal variability in the reef inorganic carbon levels is strongly influenced by seasonal variability in offshore source water, as indicated by A_T in Figure 6. During the summer "acidic" conditions, A_T was near its highest level (Table 1), offsetting the pH effect on $[CO_3^{2-}]$ (Figure 3g). For example, if the mean winter A_T is combined with the mean summer pH (Table 1), $[CO_3^{2-}]$ is near 210 μmol kg^{-1}; whereas, the mean summer A_T and pH estimate that $[CO_3^{2-}]$ is $\sim$230 μmol kg^{-1}, approximately a 10% difference (T and S were held constant in this calculation). $[CO_3^{2-}]$ would be even higher in the summer except that summer net calcification, as discussed above, reduces the open ocean source water A_T significantly. Solubility changes (changes in K_{sp}) were of comparatively lesser importance between winter and summer, with the higher mean summer temperature (lower solubility) and higher mean summer salinity (higher solubility) changing Ω_{Ar} by +1.5% and −2.1%, respectively, nearly offsetting each other.

[31] In the fall, mean temperature, pCO_2 and pH are comparable to summer levels (Table 1) indicating similar contributions from calcification and respiration; however, saturation states are lower than in either winter or summer (Figure 3 and Table 1). The $[CO_3^{2-}]$ dropped from summer to fall due to a decrease in A_T and DIC driven by rain and local freshwater runoff (Figure 3g). The change in $[CO_3^{2-}]$ alone dropped Ω_{Ar} by 12.2% with an additional 5.6% decrease due to a decrease in $[Ca^{2+}]$ (lower salinity, Figure 2b). The decrease in salinity also increased Ω_{Ar} by 7.4% through a decrease in K_{sp}. Consequently, Ω_{Ar} is lower in the fall largely due to salinity-driven decreases in $[CO_3^{2-}]$ and $[Ca^{2+}]$.

[32] *Gledhill et al.* [2008] mapped Ω_{Ar} for Caribbean waters using empirical relationships for pCO_2 and A_T. They concluded that changes in temperature and freshwater input are the most important processes controlling seasonal Ω_{Ar} variability in the southern Caribbean. Their estimated Ω_{Ar} had a higher mean and smaller seasonal range ($\sim$3.95–4.10 for 2006) compared to our results (Table 1). Because their Ω_{Ar} values were derived from open ocean variability, they do not capture the large contributions from organic matter respiration and other local events, such as freshwater runoff and calcification that tend to decrease Ω_{Ar}. In the summer and winter there are times that our saturation states are close to the mean values in *Gledhill et al.* [2008]; however, the diel cycle, particularly in the winter, brings the aragonite saturation state close to 3 for short periods (Figures 3 and 7).

5. Future Implications

[33] Atmospheric CO_2 values are expected to continue to rise from current values of $\sim$390 μatm, possibly up to 500 μatm or higher by 2035–2065 [*Meehl et al.*, 2007], which will intensify ocean acidification. To estimate the effect of this increase on the pH and saturation state of the reef, we increased the measured pCO_2 from each season and calculated the expected pH and saturation states under

Table 5. Total and Longest Continuous Exposure to Saturation States ≤3.0 in Hours for Preindustrial, Current and Future pCO_2 Levels[a]

Mean pCO_2 Level	Exposure	Summer 2007	Winter 2008	Fall 2008
280 μatm	total	0	0	0
	longest continuous	0	0	0
Current conditions	total	0	9 (0.6%)	69 (4.4%)
	longest continuous	0	3	15
500 μatm	total	974 (71%)	814 (56%)	922 (58%)
	longest continuous	119	24	92

[a]The percentage of total time is shown in parentheses.

these conditions. The calculations used a constant A_T of 2250 μmol kg^{-1} at the measured reef temperature and salinity. A 120 μatm increase in pCO_2 ($\sim$500 μatm total) decreases pH by 0.11, 0.12 and 0.08 for the summer, winter and fall seasons, respectively, relative to contemporary values. The Ω_{Ar} decreases by 0.99, 0.89 and 0.40 for the three seasons (Figure 8). *Kleypas and Langdon* [2006] show that the response to acidification varies widely among different coral species, but that on average a 1.0 unit change in Ω_{Ar} results in a $\sim$20% decrease in calcification rate. Calcification rates on Media Luna reef are therefore likely to be significantly reduced by ocean acidification within the next 30–50 years. Long duration exposure to low Ω_{Ar} levels could intensify these effects. Ω_{Ar} is projected to be less than 3.0 from 50 to 70% of the time if pCO_2 increases to 500 μatm (Table 5). In contrast, there was no exposure to $<$3.0 levels for preindustrial waters (Table 5). Mean Ω_{Ar} will be at the lowest recorded levels for all reefs ($\sim$2.5) when atmospheric pCO_2 reaches 655 μatm.

[34] Our in situ sensors have made it possible to accurately characterize pH and saturation states on coral reefs and have shown that the reef currently experiences large seasonal and diel variability. Similar studies are needed to characterize saturation state variability on other reefs. These studies should be combined with field measurements of calcification rates to verify laboratory and mesocosm data that show declining rates of calcification with decreasing Ω_{Ar} [*Kleypas and Langdon*, 2006]. Lastly, pH and pCO_2 data can be used to develop regional geochemical models, such as the Caribbean saturation state model of *Gledhill et al.* [2008], which often do not contain enough data for coastal and reef ecosystems to make accurate predictions in these areas.

[35] **Acknowledgments.** We thank Cory Beatty from the University of Montana and Helena Antoun, Valentine Hensley and Belitza Brocco from the University of Puerto Rico, Mayagüez for their assistance. We greatly appreciate the in-depth comments provided by two anonymous reviewers. We also thank the NOAA ICON program for data and mooring support. Funding for this research was provided by the National Science Foundation (grants OCE-0836807 and OCE-0628569) and a NASA Montana Space Grant Consortium Fellowship to S.E.C.G.

References

Acevedo, R., J. Morelock, and R. A. Olivieri (1989), Modification of coral reef zonation by terrigenous sediment stress, *Palaios*, *4*, 92–100, doi:10.2307/3514736.

Bates, N. R., L. Samuels, and L. Merlivat (2001), Biogeochemical and physical factors influencing seawater fCO_2 and air-sea CO_2 exchange on the Bermuda coral reef, *Limnol. Oceanogr.*, *46*(4), 833–846, doi:10.4319/lo.2001.46.4.0833.

Bates, N. R., A. Amat, and A. J. Andersson (2010), Feedbacks and responses of coral calcification on the Bermuda reef system to seasonal changes in biological processes and ocean acidification, *Biogeosciences*, *7*, 2509–2530, doi:10.5194/bg-7-2509-2010.

Borges, A. V., S. Djenidi, G. Lacroix, J. Théate, B. Delille, and M. Frankignoulle (2003), Atmospheric CO_2 flux from mangrove surrounding waters, *Geophys. Res. Lett.*, *30*(11), 1558, doi:10.1029/2003GL017143.

Borges, A. V., B. Delille, L.-S. Schiettecatte, F. Gazeau, G. Abril, and M. Frankignoulle (2004), Gas transfer velocities of CO_2 in three European estuaries (Randers Fjord, Scheldt, and Thames), *Limnol. Oceanogr.*, *49*, 1630–1641, doi:10.4319/lo.2004.49.5.1630.

Borges, A. V., B. Delille, and M. Frankignoulle (2005), Budgeting sinks and sources of CO_2 in the coastal ocean: Diversity of ecosystems counts, *Geophys. Res. Lett.*, *32*, L14601, doi:10.1029/2005GL023053.

Bouillon, S., F. Dehairs, B. Velimirov, G. Abril, and A. V. Borges (2007), Dynamics of organic and inorganic carbon across contiguous mangrove and seagrass systems (Gazi Bay, Kenya), *J. Geophys. Res.*, *112*, G02018, doi:10.1029/2006JG000325.

Byrne, R. H., and J. A. Breland (1989), High precision multiwavelength pH determinations in seawater using cresol red, *Deep Sea Res., Part A*, *36*(5), 803–810, doi:10.1016/0198-0149(89)90152-0.

Caldeira, K., and M. E. Wickett (2003), Oceanography: Anthropogenic carbon and ocean pH, *Nature*, *425*(6956), 365, doi:10.1038/425365a.

Cao, L., K. Caldeira, and A. K. Jain (2007), Effects of carbon dioxide and climate change on ocean acidification and carbonate mineral saturation, *Geophys. Res. Lett.*, *34*, L05607, doi:10.1029/2006GL028605.

Chen, C.-T. A., and A. V. Borges (2009), Reconciling opposing views on carbon cycling in the coastal ocean: Continental shelves as sinks and near-shore ecosystems as sources of atmospheric CO_2, *Deep Sea Res., Part II*, *56*, 578–590, doi:10.1016/j.dsr2.2009.01.001.

Cintrón, G., A. E. Lugo, D. J. Pool, and G. Morris (1978), Mangroves of arid environments in Puerto Rico and adjacent islands, *Biotropica*, *10*(2), 110–121, doi:10.2307/2388013.

Clayton, T. D., and R. H. Byrne (1993), Spectrophotometric seawater pH measurements: Total hydrogen ion concentration scale calibration of *m*-cresol purple and at-sea results, *Deep Sea Res., Part I*, *40*(10), 2115–2129.

Corredor, J. E., and J. M. Morell (2001), Seasonal variation of physical and biogeochemical features in eastern Caribbean surface water, *J. Geophys. Res.*, *106*(C3), 4517–4525.

Culberson, C. H., and S. Huang (1987), Automated amperometric oxygen titration, *Deep Sea Res., Part A*, *34*, 875–880, doi:10.1016/0198-0149(87)90042-2.

Cullison Gray, S. E., M. D. DeGrandpre, T. S. Moore, T. R. Martz, G. E. Friederich, and K. S. Johnson (2011), Applications of *in situ* pH measurements for inorganic carbon calculations, *Mar. Chem.*, *125*, 82–90, doi:10.1016/j.marchem.2011.02.005.

DeGrandpre, M. D., T. R. Hammar, S. P. Smith, and F. L. Sayles (1995), In situ measurements of seawater pCO_2, *Limnol. Oceanogr.*, *40*, 969–975, doi:10.4319/lo.1995.40.5.0969.

DelValls, T. A., and A. G. Dickson (1998), The pH of buffers based on 2-amino-2-hydroxymethyl-1,3-propanediol ('tris') in synthetic sea water, *Deep Sea Res., Part I*, *45*, 1541–1554, doi:10.1016/S0967-0637(98)00019-3.

Dickson, A. G. (1990), Standard potential of the (AgCl(s) + $^1/_2H_2$ (g) = Ag(s) + HCl(aq)) cell and the dissociation constant of bisulfate ion in synthetic sea water from 273.15 to 318.15 K, *J. Chem. Thermodyn.*, *22*, 113–127.

Dickson, A. G., and F. J. Millero (1987), A comparison of the equilibrium constants for the dissociation of carbonic acid in seawater media, *Deep Sea Res., Part A*, *34*(10), 1733–1743, doi:10.1016/0198-0149(87)90021-5.

Dickson, A. G., J. D. Afghan, and G. C. Anderson (2003), Reference materials for oceanic CO_2 analysis: A method for the certification of total alkalinity, *Mar. Chem.*, *80*(2–3), 185–197, doi:10.1016/S0304-4203(02)00133-0.

Dickson, A. G., C. L. Sabine, and J. R. Christian (Eds.) (2007), *Guide to Best Practices for Ocean CO_2 Measurements*, *PICES Spec. Publ.*, vol. 3, 191 pp., U.S. Dep. of Energy, Washington, D. C.

Drupp, P., E. H. De Carlo, F. T. Mackenzie, P. Bienfang, and C. L. Sabine (2011), Nutrient inputs, phytoplankton response, and CO_2 variations in a semi-enclosed subtropical embayment, Kaneohe Bay, Hawaii, *Aquat. Geochem.*, *17*, 473–498, doi:10.1007/s10498-010-9115-y.

Emerson, S., C. Sabine, M. F. Cronin, R. Feely, S. E. Cullison Gray, and M. DeGrandpre (2011), Quantifying the flux of $CaCO_3$ and organic carbon from the surface ocean using in situ measurements of O_2, N_2, pCO_2, and pH, *Global Biogeochem. Cycles*, *25*, GB3008, doi:10.1029/2010GB003924.

Fabry, V. J., B. A. Seibel, R. A. Feely, and J. C. Orr (2008), Impacts of ocean acidification on marine fauna and ecosystem processes, *ICES J. Mar. Sci.*, *65*(3), 414–432, doi:10.1093/icesjms/fsn048.

Fagan, K. E., and F. T. Mackenzie (2007), Air-sea CO_2 exchange in a subtropical estuarine-coral reef system, Kaneohe Bay, Oahu, Hawaii, *Mar. Chem.*, *106*, 174–191, doi:10.1016/j.marchem.2007.01.016.

Feely, R. A., C. L. Sabine, K. Lee, W. Berelson, J. Kleypas, V. J. Fabry, and F. J. Millero (2004), Impact of anthropogenic CO_2 on the $CaCO_3$ system in the oceans, *Science*, *305*(5682), 362–366, doi:10.1126/science.1097329.

Frankignoulle, M., J. P. Gattuso, R. Biondo, I. Bourge, G. Copin-Montégut, and M. Pichon (1996), Carbon fluxes in coral reefs. II. Eulerian study of inorganic carbon dynamics and measurement of air-sea CO_2 exchanges, *Mar. Ecol. Prog. Ser.*, *145*(1–3), 123–132, doi:10.3354/meps145123.

García, J. R., C. Schmitt, C. Heberer, and A. Winter (1998), La Parguera, Puerto Rico, USA, in *CARICOMP—Caribbean Coral Reef, Seagrass and Mangrove Sites*, *Coastal Reg. Small Isl. Pap.*, vol. 3, pp. 187–193, UNESCO, Paris. [Available at www.unesco.org/csi/pub/papers/papers3.htm.]

Gattuso, J.-P., M. Frankignoulle, and S. V. Smith (1999), Measurement of community metabolism and significance in the coral reef CO_2 source-sink debate, *Proc. Natl. Acad. Sci. U. S. A.*, *96*(23), 13,017–13,022, doi:10.1073/pnas.96.23.13017.

Gledhill, D. K., R. Wanninkhof, F. J. Millero, and M. Eakin (2008), Ocean acidification of the Greater Caribbean Region 1996–2006, *J. Geophys. Res.*, *113*, C10031, doi:10.1029/2007JC004629.

Ho, D. T., C. S. Law, M. J. Smith, P. Schlosser, M. Harvey, and P. Hill (2006), Measurements of air-sea gas exchange at high wind speeds in the Southern Ocean: Implications for global parameterizations, *Geophys. Res. Lett.*, *33*, L16611, doi:10.1029/2006GL026817.

Jokiel, P. L., K. S. Rodgers, I. B. Kuffner, A. J. Andersson, E. F. Cox, and F. T. Mackenzie (2008), Ocean acidification and calcifying reef organisms: A mesocosm investigation, *Coral Reefs*, *27*, 473–483, doi:10.1007/s00338-008-0380-9.

Kawahata, H., I. Yukino, and A. Suzuki (2000), Terrestrial influences on the Shiraho fringing reef, Ishigaki Island, Japan: High carbon input relative to phosphate, *Coral Reefs*, *19*, 172–178, doi:10.1007/s003380000093.

Kayanne, H., H. Hata, S. Kudo, H. Yamano, A. Watanabe, Y. Ikeda, K. Nozaki, K. Kato, A. Negishi, and H. Saito (2005), Seasonal and bleaching-induced changes in coral reef metabolism and CO_2 flux, *Global Biogeochem. Cycles*, *19*, GB3015, doi:10.1029/2004GB002400.

Kleypas, J. A., and C. Langdon (2006), Coral reefs and changing seawater carbonate chemistry, in *Coral Reefs and Climate Change: Science and Management*, *Coastal Estuarine Stud.*, vol. 61, edited by J. T. Phinney et al., pp. 73–110, AGU, Washington, D. C., doi:10.1029/61CE06.

Kleypas, J. A., K. R. N. Anthony, and J.-P. Gattuso (2011), Coral reefs modify their seawater carbon chemistry—Case study from a barrier reef (Moorea, French Polynesia), *Global Change Biol.*, *17*, 3667–3678, doi:10.1111/j.1365-2486.2011.02530.x.

Koné, Y. J.-M., and A. V. Borges (2008), Dissolved inorganic carbon dynamics in the waters surrounding forested mangroves of the Ca Mau Province (Vietnam), *Estuarine Coastal Shelf Sci.*, *77*, 409–421, doi:10.1016/j.ecss.2007.10.001.

Langdon, C., and M. J. Atkinson (2005), Effect of elevated pCO_2 on photosynthesis and calcification of corals and interactions with seasonal change in temperature/irradiance and nutrient enrichment, *J. Geophys. Res.*, *110*, C09S07, doi:10.1029/2004JC002576.

Langdon, C., T. Takahashi, C. Sweeney, D. Chipman, J. Goddard, F. Marubini, H. Aceves, H. Barnett, and M. J. Atkinson (2000), Effect of calcium carbonate saturation state on the calcification rate of an experimental coral reef, *Global Biogeochem. Cycles*, *14*(2), 639–654, doi:10.1029/1999GB001195.

Langdon, C., W. S. Broecker, D. E. Hammond, E. Glenn, K. Fitzsimmons, S. G. Nelson, T.-H. Peng, I. Hajdas, and G. Bonani (2003), Effect of elevated CO_2 on the community metabolism of an experimental coral reef, *Global Biogeochem. Cycles*, *17*(1), 1011, doi:10.1029/2002GB001941.

Large, W. G., J. Morzel, and G. B. Crawford (1995), Accounting for surface wave distortion of the marine wind profile in low-level ocean storms wind measurements, *J. Phys. Oceanogr.*, *25*, 2959–2971.

Leclercq, N., J.-P. Gattuso, and J. Jaubert (2000), CO_2 partial pressure controls the calcification rate of a coral community, *Global Change Biol.*, *6*, 329–334, doi:10.1046/j.1365-2486.2000.00315.x.

Lee, K., L. T. Tong, F. J. Millero, C. L. Sabine, A. G. Dickson, C. Goyet, G.-H. Park, R. Wanninkhof, R. A. Feely, and R. M. Key (2006), Global relationships of total alkalinity with salinity and temperature in surface waters of the world's oceans, *Geophys. Res. Lett.*, *33*, L19605, doi:10.1029/2006GL027207.

Liu, X., Z. A. Wang, R. H. Byrne, E. A. Kaltenbacher, and R. E. Bernstein (2006), Spectrophotometric measurements of pH in-situ: Laboratory and field evaluations of instrumental performance, *Environ. Sci. Technol.*, *40*, 5036–5044, doi:10.1021/es0601843.

Manzello, D. P. (2010), Ocean acidification hotspots: Spatiotemporal dynamics of the seawater CO_2 system of eastern Pacific coral reefs, *Limnol. Oceanogr.*, *55*, 239–248, doi:10.4319/lo.2010.55.1.0239.

Martz, T. R., J. J. Carr, C. R. French, and M. D. DeGrandpre (2003), A submersible autonomous sensor for spectrophotometric pH measurements of natural waters, *Anal. Chem.*, *75*, 1844–1850, doi:10.1021/ac020568l.

Meehl, G. A., et al. (2007), Global climate projections, in *Climate Change 2007: The Scientific Basis: Contribution of Working Group I to the Fourth Assessment Report of the Intergovernmental Panel on Climate Change*, pp. 747–845, Cambridge Univ. Press, New York.

Mehrbach, C., C. H. Culberson, J. E. Hawley, and R. M. Pytkowicz (1973), Measurement of the apparent dissociation constants of carbonic acid in seawater at atmospheric pressure, *Limnol. Oceanogr.*, *18*, 897–907, doi:10.4319/lo.1973.18.6.0897.

Nakano, Y., H. Kimoto, S. Watanabe, K. Harada, and Y. W. Watanabe (2006), Simultaneous vertical measurements of *in situ* pH and CO_2 in the sea using spectrophotometric profilers, *J. Oceanogr.*, *62*, 71–81, doi:10.1007/s10872-006-0033-y.

Olsen, A., J. A. Triñanes, and R. Wanninkhof (2004), Sea-air flux of CO_2 in the Caribbean Sea estimated using in situ and remote sensing data, *Remote Sens. Environ.*, *89*, 309–325, doi:10.1016/j.rse.2003.10.011.

Orr, J. C., et al. (2005), Anthropogenic ocean acidification over the twenty-first century and its impact on calcifying organisms, *Nature*, *437*(7059), 681–686, doi:10.1038/nature04095.

Pierrot, D., E. Lewis, and D. W. R. Wallace (2006), MS Excel program developed for CO2 system calculations, *Rep. ORNL/CDIAC-105a*, Carbon Dioxide Inf. Anal. Cent., Oak Ridge Natl. Lab., U.S. Dep. of Energy, Oak Ridge, Tenn., doi:10.3334/CDIAC/otg.CO2SYS_XLS_CDIAC105a.

Sabine, C. L., R. A. Feely, R. Wanninkhof, T. Takahashi, S. Khatiwala, and G.-H. Park (2011), The global ocean carbon cycle, *Bull. Am. Meteorol. Soc.*, *92*, suppl., S100–S105.

Santos, I. R., R. N. Glud, D. Maher, D. Erler, and B. D. Eyre (2011), Diel coral reef acidification driven by porewater advection in permeable carbonate sands, Heron Island, Great Barrier Reef, *Geophys. Res. Lett.*, *38*, L03604, doi:10.1029/2010GL046053.

Seidel, M. P., M. D. DeGrandpre, and A. G. Dickson (2008), A sensor for in situ indicator-based measurements of seawater pH, *Mar. Chem.*, *109*(1–2), 18–28, doi:10.1016/j.marchem.2007.11.013.

Shamberger, K. E. F., R. A. Feely, C. L. Sabine, M. J. Atkinson, E. H. DeCarlo, F. T. Mackenzie, P. S. Drupp, and D. A. Butterfield (2011), Calcification and organic production on a Hawaiian coral reef, *Mar. Chem.*, *127*, 64–75, doi:10.1016/j.marchem.2011.08.003.

Silverman, J., B. Lazar, and J. Erez (2007), Effect of aragonite saturation, temperature, and nutrients on the community calcification rate of a coral reef, *J. Geophys. Res.*, *112*, C05004, doi:10.1029/2006JC003770.

Solomon, S., G.-K. Plattner, R. Knutti, and P. Friedlingstein (2009), Irreversible climate change due to carbon dioxide emissions, *Proc. Natl. Acad. Sci. U. S. A.*, *106*(6), 1704–1709, doi:10.1073/pnas.0812721106.

Takahashi, T., et al. (2002), Global sea-air CO_2 flux based on climatological surface ocean pCO_2, and seasonal biological and temperature effects, *Deep Sea Res., Part II*, *49*, 1601–1622, doi:10.1016/S0967-0645(02)00003-6.

The Royal Society (2005), Ocean acidification due to increasing atmospheric carbon dioxide, policy document, London.

Winter, A., R. S. Appeldoorn, A. Bruckner, E. H. Williams Jr., and C. Goenaga (1998), Sea surface temperatures and coral reef bleaching off La Parguera, Puerto Rico (northeastern Caribbean Sea), *Coral Reefs*, *17*, 377–382, doi:10.1007/s003380050143.

Yates, K. K., and R. B. Halley (2006), CO_3^{2-} concentration and pCO_2 thresholds for calcification and dissolution on the Molokai reef flat, Hawaii, *Biogeosciences*, *3*(3), 357–369, doi:10.5194/bg-3-357-2006.